



The antibiotic furagin and its derivatives are isoform-selective human carbonic anhydrase inhibitors

Aleksandrs Pustenko, Alessio Nocentini, Paola Gratteri, Alessandro Bonardi, Igor Vozny, Raivis Žalubovskis & Claudiu T. Supuran

To cite this article: Aleksandrs Pustenko, Alessio Nocentini, Paola Gratteri, Alessandro Bonardi, Igor Vozny, Raivis Žalubovskis & Claudiu T. Supuran (2020) The antibiotic furagin and its derivatives are isoform-selective human carbonic anhydrase inhibitors, Journal of Enzyme Inhibition and Medicinal Chemistry, 35:1, 1011-1020, DOI: [10.1080/14756366.2020.1752201](https://doi.org/10.1080/14756366.2020.1752201)

To link to this article: <https://doi.org/10.1080/14756366.2020.1752201>



© 2020 The Author(s). Published by Informa UK Limited, trading as Taylor & Francis Group.



[View supplementary material](#)



Published online: 16 Apr 2020.



[Submit your article to this journal](#)



[View related articles](#)



[View Crossmark data](#)

RESEARCH PAPER



The antibiotic furagin and its derivatives are isoform-selective human carbonic anhydrase inhibitors

Aleksandrs Pustenko^{a,b}, Alessio Nocentini^{c,d}, Paola Gratteri^d, Alessandro Bonardi^{c,d}, Igor Vozny^a, Raivis Žalubovskis^{a,b} and Claudiu T. Supuran^c 

^aLatvian Institute of Organic Synthesis, Riga, Latvia; ^bInstitute of Technology of Organic Chemistry, Faculty of Materials Science and Applied Chemistry, Riga Technical University, Riga, Latvia; ^cDepartment of NEUROFARBA, Section of Pharmaceutical and Nutraceutical Sciences, University of Florence, Firenze, Italy; ^dDepartment of NEUROFARBA, Section of Pharmaceutical and Nutraceutical Sciences, Laboratory of Molecular Modeling Cheminformatics & QSAR, University of Florence, Firenze, Italy

ABSTRACT

The clinically used antibiotic Furagin and its derivatives possess inhibitory activity on human (h) carbonic anhydrases (CA, EC 4.2.1.1), some of which are highly expressed in various tissues and malignancies (hCA IX/XII). Furagin exhibited good hCA IX and XII inhibition with K_i s of 260 and 57 nM, respectively. It does not inhibit off-target CA I and poorly inhibited CA II ($K_i = 9.6 \mu\text{M}$). Some synthesised Furagin derivatives with aminohydantoin moieties as zinc binding group exhibited weak inhibition of CA I/II, and good inhibition of CA IX/XII with K_i s ranging from 350 to 7400 and 150 to 5600 nM, respectively. Docking and molecular dynamics simulations suggest that selectivity for the cancer-associated CA IX/XII over CA II is due to strong H-bond interactions in CA IX/XII, involving the tail orientated towards hydrophobic area of the active site. These results suggest a possible drug repurposing of Furagin as anti-cancer agent.

ARTICLE HISTORY

Received 6 March 2020
Revised 31 March 2020
Accepted 1 April 2020

KEYWORDS

Carbonic anhydrase inhibitors; molecular dynamics; furagin; hydantoin; synthesis

1. Introduction

Carbonic anhydrases (CAs, EC 4.2.1.1) are ubiquitous metalloenzymes, being encoded by at least eight different genetic families, which have been found in organisms all over the phylogenetic tree^{1–10}. CAs catalyse a crucial physiologic reaction, where by hydration of CO₂ is formed a weak base (bicarbonate) and a strong acid (hydronium ions). These enzymes are involved in a multitude of physiologic processes, starting with pH regulation and ending with metabolism^{1–3,7–10,11–22}.

CAs are also involved in various pathological processes and therefore are drug targets for decades, with their inhibitors having pharmacological applications in many fields^{1–3,7–19}. The primary sulphonamides were discovered as CA inhibitors (CAIs) already in the 40s, and most of the drugs that were launched in the next decades as diuretics, antiepileptics, or antiglaucoma agents targeting CAs belonged to this class of compounds^{1–3,7–19}. Although highly potent as CAIs^{1–3}, the sulphonamides generally non-selectively inhibit most α -CA isoforms present in humans and mammals in general^{1–3} as well as CAs from the other genetic families (β -, γ -, δ -, ζ -, η -, θ - and ι -CAs)^{4–19}, therefore alternative, isoform selective CAI classes were searched. A multitude of new chemotypes as well as novel CA inhibition mechanisms were reported in the last decade^{1–3,11–14,23–30}.





That has highly enriched our understanding of these enzymes and also allowed obtaining of isoform-selective CAIs targeting physiologically relevant isoforms^{11–14,23–27}. Among the new chemotypes, which also exhibited the highest levels of isoform


selectivity, were the coumarins²⁷, the sulfocoumarins^{23–26} and their congeners, homosulfocoumarins (3H-1,2-benzoxathiepine 2,2-dioxides)³¹, and saccharin derivatives^{32–34}. Considering the fact that this last chemotype was somewhat chemically similar to hydantoin (imidazolidine-2,4-dione) that may serve as zinc binding group (ZBG) we investigated clinically used antibiotic **Furagin** (Figure 1), also known under names Furazidine, Furamags or Furazidin³⁵, that contains hydantoin moiety, as well as newly prepared its derivatives.

2. Materials and methods

2.1. Chemical syntheses – general

Reagents, starting materials and solvents were obtained from commercial sources and used as received. Thin-layer chromatography was performed on silica gel, spots were visualised with UV light (254 and 365 nm). Melting points were determined on an OptiMelt automated melting point system. IR spectra were recorded on Shimadzu FTIR IR Prestige-21 spectrometer. NMR spectra were recorded on Bruker Avance Neo (400 MHz) spectrometer with chemical shifts values (δ) in ppm relative to TMS using the residual DMSO-d₆ signal (¹H 2.50; ¹³C 39.52) or CDCl₃ signal (¹H 7.26; ¹³C 77.16) as an internal standard, or D₂O signal and dioxane (¹H 4.79; ¹³C 67.19). High-resolution mass spectra (HRMS) were recorded on a mass spectrometer with a Q-TOF micro mass

CONTACT Raivis Žalubovskis  raivis@osi.lv  Riga Technical University, Riga, Latvia; Claudiu T. Supuran  claudiu.supuran@unifi.it  University of Florence, Firenze, Italy

 Supplemental data for this article can be accessed [here](#).

© 2020 The Author(s). Published by Informa UK Limited, trading as Taylor & Francis Group.

This is an Open Access article distributed under the terms of the Creative Commons Attribution License (<http://creativecommons.org/licenses/by/4.0/>), which permits unrestricted use, distribution, and reproduction in any medium, provided the original work is properly cited.

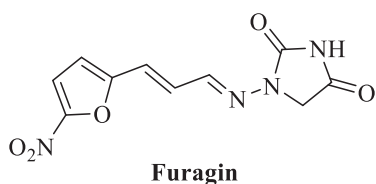


Figure 1. Structure of Furagin.

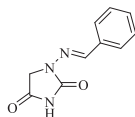
analyser using the ESI technique. Examples of spectral data are furnished in the Supporting Information to the article.

2.2. General procedure for compound 2–17 synthesis

To a solution of 1-aminoimidazolidine-2,4-dione hydrochloride (**1**) (1.0 eq.) in EtOH (15 ml per 1 mmol of compound **1**) appropriate aldehyde (1.05 eq.) was added. The resulting mixture was stirred at room temperature overnight.

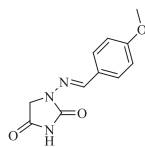
The solvent was removed under vacuum and the crude product was re-crystallized from EtOH to afford product.

2.2.1. 1-(Benzylideneamino)-imidazolidine-2,4-dione (**2**)³⁶



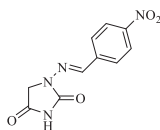
Compound **2** was prepared according to the general procedure from compound **1** (0.5 g; 3.30 mmol) and benzaldehyde (0.35 ml; 3.46 mmol) as white solid (0.60 g; 90%). Mp 252 – 253 °C. IR (film, cm^{-1}) ν_{max} = 1778 (C=O), 1717 (C=O); ^1H NMR (400 MHz, DMSO- d_6) δ = 4.36 (s, 2H), 7.38–7.48 (m, 3H), 7.68–7.72 (m, 2H), 7.80 (s, 1H), 11.25 (s, 1H) ppm ^{13}C NMR (100 MHz, DMSO- d_6) δ = 48.9, 126.8, 128.8, 129.8, 134.3, 143.0, 153.4, 169.0 ppm HRMS (ESI) $[\text{M} + \text{H}]^+$: m/z calcd for ($\text{C}_{10}\text{H}_{10}\text{N}_3\text{O}_2$) 204.0773. Found 204.0783.

2.2.2. 1-((4-Methoxybenzylidene)amino)imidazolidine-2,4-dione (**3**)



Compound **3** was prepared according to the general procedure from compound **1** (0.5 g; 3.30 mmol) and 4-methoxybenzaldehyde (0.42 ml; 3.46 mmol) as white solid (0.62 g; 80%). Mp 242 – 244 °C. IR (film, cm^{-1}) ν_{max} = 1768 (C=O), 1718 (C=O); ^1H NMR (400 MHz, DMSO- d_6) δ = 3.80 (s, 3H), 4.33 (s, 2H), 6.99–7.04 (m, 2H), 7.62–7.66 (m, 2H), 7.75 (s, 1H), 11.18 (s, 1H) ppm ^{13}C NMR (100 MHz, DMSO- d_6) δ = 48.9, 55.3, 114.3, 126.9, 128.4, 142.9, 153.4, 160.6, 169.1 ppm HRMS (ESI) $[\text{M} + \text{H}]^+$: m/z calcd for ($\text{C}_{11}\text{H}_{12}\text{N}_3\text{O}_3$) 234.0879. Found 234.0885.

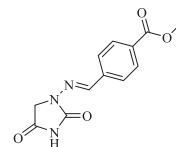
2.2.3. 1-((4-Nitrobenzylidene)amino)imidazolidine-2,4-dione (**4**)³⁷



Compound **4** was prepared according to the general procedure

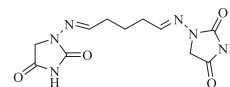
from compound **1** (0.5 g; 3.30 mmol) and 4-nitrobenzaldehyde (0.52 g; 3.46 mmol) as yellowish solid (0.68 g; 82%). Mp 280 °C dec. IR (film, cm^{-1}) ν_{max} = 1780 (C=O), 1714 (C=O); ^1H NMR (400 MHz, DMSO- d_6) δ = 4.38 (s, 2H), 7.90–7.96 (m, 3H), 8.28–8.33 (m, 2H), 11.39 (s, 1H) ppm ^{13}C NMR (100 MHz, DMSO- d_6) δ = 49.1, 124.2, 127.7, 140.6, 140.7, 147.6, 153.4, 168.9 ppm HRMS (ESI) $[\text{M} + \text{H}]^+$: m/z calcd for ($\text{C}_{10}\text{H}_9\text{N}_4\text{O}_4$) 249.0624. Found 249.0616.

2.2.4. Methyl 4-(((2,4-dioxoimidazolidin-1-yl)imino)methyl)benzoate (**5**)



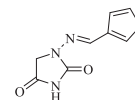
Compound **5** was prepared according to the general procedure from compound **1** (0.5 g; 3.30 mmol) and methyl 4-formylbenzoate (0.57 g; 3.46 mmol) as white solid (0.82 g; 95%). Mp 280 °C dec. IR (film, cm^{-1}) ν_{max} = 1763 (C=O), 1717 (C=O); ^1H NMR (400 MHz, DMSO- d_6) δ = 3.86 (s, 3H), 4.37 (s, 2H), 7.80–7.87 (m, 3H), 8.00–8.05 (m, 2H), 11.33 (s, 1H) ppm ^{13}C NMR (100 MHz, DMSO- d_6) δ = 49.0, 52.2, 127.0, 129.7, 130.2, 138.8, 141.6, 153.4, 165.9, 168.9 ppm HRMS (ESI) $[\text{M} + \text{H}]^+$: m/z calcd for ($\text{C}_{12}\text{H}_{12}\text{N}_3\text{O}_4$) 262.0828. Found 262.0834.

2.2.5. 1,1'-((Pentane-1,5-diylidene)bis(azaneylylidene))bis(imidazolidine-2,4-dione) (**6**)



Compound **6** was prepared according to the general procedure from compound **1** (0.5 g; 3.30 mmol) and glutaraldehyde 50 wt % solution in H_2O (0.31 ml; 3.46 mmol) as white solid (0.49 g; 50%). Mp 237 °C dec. IR (film, cm^{-1}) ν_{max} = 1768 (C=O), 1734 (C=O); ^1H NMR (400 MHz, DMSO- d_6) δ = 1.72 (p, 2H, J = 7.4 Hz), 2.28–2.36 (m, 4H), 4.17 (s, 4H), 7.06 (t, 2H, J = 5.2 Hz), 11.07 (s, 2H) ppm ^{13}C NMR (100 MHz, DMSO- d_6) δ = 23.1, 31.3, 48.5, 146.7, 153.4, 169.1 ppm HRMS (ESI) $[\text{M} + \text{Na}]^+$: m/z calcd for ($\text{C}_{11}\text{H}_{14}\text{N}_6\text{O}_4\text{Na}$) 317.0974. Found 317.0978.

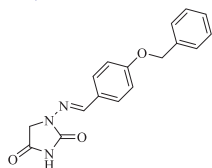
2.2.6. 1-((Furan-3-ylmethylene)amino)imidazolidine-2,4-dione (**7**)



Compound **7** was prepared according to the general procedure from compound **1** (0.5 g; 3.30 mmol) and 3-furaldehyde (0.33 g; 3.46 mmol) as yellowish solid (0.57 g; 89%). Mp 235 °C dec. IR (film, cm^{-1}) ν_{max} = 1780 (C=O), 1714 (C=O);

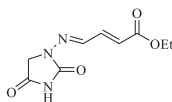
^1H NMR (400 MHz, DMSO- d_6) δ = 4.30 (s, 2H), 6.74–6.76 (m, 1H), 7.73–7.77 (m, 2H), 8.05–8.07 (m, 1H), 11.18 (s, 1H) ppm ^{13}C NMR (100 MHz, DMSO- d_6) δ = 48.8, 107.0, 122.5, 136.1, 144.8, 144.9, 153.3, 169.1 ppm HRMS (ESI) $[\text{M} + \text{H}]^+$: m/z calcd for ($\text{C}_8\text{H}_8\text{N}_3\text{O}_3$) 194.0566. Found 194.0570.

2.2.7. 1-((4-(Benzyloxy)benzylidene)amino)imidazolidine-2,4-dione (8)



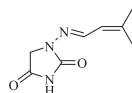
Compound **8** was prepared according to the general procedure from compound **1** (0.5 g; 3.30 mmol) and 4-benzyloxybenzaldehyde (0.73 g; 3.46 mmol) as white solid (0.92 g; 90%). Mp 258–260 °C. IR (film, cm^{-1}) $\nu_{\text{max}}=1790$ (C=O), 1730 (C=O); ^1H NMR (400 MHz, DMSO-d_6) $\delta=4.33$ (s, 2H), 5.15 (s, 2H), 7.07–7.12 (m, 2H), 7.31–7.36 (m, 1H), 7.37–7.43 (m, 2H), 7.44–7.49 (m, 2H), 7.62–7.67 (m, 2H), 7.75 (s, 1H), 11.19 (s, 1H) ppm ^{13}C NMR (100 MHz, DMSO-d_6) $\delta=48.9$, 69.4, 115.1, 127.1, 127.8, 127.9, 128.4, 128.5, 136.8, 142.8, 153.4, 159.7, 169.1 ppm HRMS (ESI) $[\text{M} + \text{H}]^+$: m/z calcd for ($\text{C}_{17}\text{H}_{16}\text{N}_3\text{O}_3$) 310.1192. Found 310.1194.

2.2.8. Ethyl (2E)-4-((2,4-dioxoimidazolidin-1-yl)imino)but-2-enoate (9)



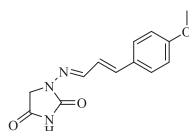
Compound **9** was prepared according to the general procedure from compound **1** (0.5 g; 3.30 mmol) and ethyl trans-4-oxo-2-butenate (0.42 ml; 3.46 mmol) as white solid (0.60 g; 81%). Mp 210–211 °C. IR (film, cm^{-1}) $\nu_{\text{max}}=1772$ (C=O), 1721 (C=O); ^1H NMR (400 MHz, DMSO-d_6) $\delta=1.24$ (t, 3H, $J=7.1$ Hz), 4.17 (q, 2H, $J=7.1$ Hz), 4.27 (s, 2H), 7.37 (d, 1H, $J=15.6$ Hz), 7.16–7.24 (m, 1H), 7.60 (d, 1H, $J=9.3$ Hz), 11.39 (s, 1H) ppm ^{13}C NMR (100 MHz, DMSO-d_6) $\delta=14.1$, 49.0, 60.4, 126.5, 140.3, 141.7, 153.2, 165.4, 168.7 ppm HRMS (ESI) $[\text{M} + \text{H}]^+$: m/z calcd for ($\text{C}_9\text{H}_{12}\text{N}_3\text{O}_4$) 226.0828. Found 226.0834.

2.2.9. 1-((3-Methylbut-2-en-1-ylidene)amino)imidazolidine-2,4-dione (10)



Compound **10** was prepared according to the general procedure from compound **1** (0.5 g; 3.30 mmol) and 3-methyl-2-butenal (0.33 ml; 3.46 mmol) as white solid (0.43 g; 72%). Mp 186–187 °C. IR (film, cm^{-1}) $\nu_{\text{max}}=1768$ (C=O), 1717 (C=O); ^1H NMR (400 MHz, DMSO-d_6) $\delta=1.84$ –1.89 (m, 6H), 4.28 (s, 2H), 5.93–5.99 (m, 1H), 7.57 (d, 1H, $J=9.5$ Hz), 11.11 (s, 1H) ppm ^{13}C NMR (100 MHz, DMSO-d_6) $\delta=18.7$, 26.2, 48.9, 121.9, 142.4, 144.3, 153.3, 169.2 ppm HRMS (ESI) $[\text{M} + \text{H}]^+$: m/z calcd for ($\text{C}_8\text{H}_{12}\text{N}_3\text{O}_2$) 182.0930. Found 182.0938.

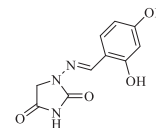
2.2.10 1-(((2e)-3-(4-methoxyphenyl)allylidene)amino)imidazolidine-2,4-dione (11)



Compound **11** was prepared according to the general procedure from compound **1** (0.5 g; 3.30 mmol) and

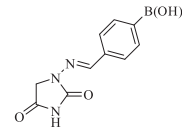
trans-4-methoxycinnamaldehyde (0.56 g; 3.46 mmol) as white solid (0.61 g; 71%). Mp 250 °C dec. IR (film, cm^{-1}) $\nu_{\text{max}}=1770$ (C=O), 1731 (C=O); ^1H NMR (400 MHz, DMSO-d_6) $\delta=3.78$ (s, 3H), 4.29 (s, 2H), 6.85–7.00 (m, 4H), 7.51–7.59 (m, 3H), 11.18 (s, 1H) ppm ^{13}C NMR (100 MHz, DMSO-d_6) $\delta=48.8$, 55.2, 114.3, 123.1, 128.5, 128.6, 138.5, 145.5, 153.3, 159.9, 169.1 ppm HRMS (ESI) $[\text{M} + \text{H}]^+$: m/z calcd for ($\text{C}_{13}\text{H}_{14}\text{N}_3\text{O}_3$) 260.1035. Found 260.1047.

2.2.11. 1-((2,4-Dihydroxybenzylidene)amino)imidazolidine-2,4-dione (12)



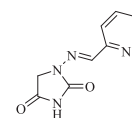
Compound **12** was prepared according to the general procedure from compound **1** (0.5 g; 3.30 mmol) and 2,4-dihydroxybenzaldehyde (0.48 g; 3.46 mmol) as white solid (0.72 g; 93%). Mp >300 °C. IR (film, cm^{-1}) $\nu_{\text{max}}=3260$ (OH), 3188 (OH), 1780 (C=O), 1717 (C=O); ^1H NMR (400 MHz, DMSO-d_6) $\delta=4.34$ (s, 2H), 6.31 (d, 1H, $J=2.3$ Hz), 6.35 (dd, 1H, $J=8.5$, 2.3 Hz), 7.33 (d, 1H, $J=8.5$ Hz), 7.90 (s, 1H), 9.90 (br s, 1H), 10.73 (s, 1H), 11.23 (br s, 1H) ppm ^{13}C NMR (100 MHz, DMSO-d_6) $\delta=48.5$, 102.6, 107.8, 110.7, 130.5, 144.0, 153.3, 158.6, 160.5, 169.1 ppm HRMS (ESI) $[\text{M} + \text{H}]^+$: m/z calcd for ($\text{C}_{10}\text{H}_{10}\text{N}_3\text{O}_4$) 236.0671. Found 236.0677.

2.2.12. 4-(((2,4-Dioxoimidazolidin-1-yl)imino)methyl)phenylboronic acid (13)

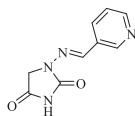


Compound **13** was prepared according to the general procedure from compound **1** (0.5 g; 3.30 mmol) and 4-formylphenylboronic acid (0.52 g; 3.46 mmol) as white solid (0.72 g; 88%). Mp >300 °C. IR (film, cm^{-1}) $\nu_{\text{max}}=3349$ (OH), 3173 (OH), 1780 (C=O), 1716 (C=O); ^1H NMR (400 MHz, DMSO-d_6) $\delta=4.37$ (s, 2H), 7.64–7.68 (m, 2H), 7.79 (s, 1H), 7.83–7.87 (m, 2H), 8.12 (s, 2H), 11.26 (s, 1H) ppm ^{13}C NMR (100 MHz, DMSO-d_6) $\delta=48.9$, 125.8, 134.5, 135.7, 136.0 (br) 143.0, 153.4, 169.1 ppm HRMS (ESI) $[\text{M} + \text{H}]^+$: m/z calcd for ($\text{C}_{10}\text{H}_{11}\text{BN}_3\text{O}_4$) 248.0843. Found 248.0847.

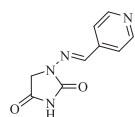
2.2.13. 1-((Pyridin-2-ylmethylene)amino)imidazolidine-2,4-dione (14)



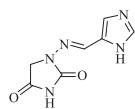
Compound **14** was prepared according to the general procedure from compound **1** (0.5 g; 3.30 mmol) and pyridine-2-carbaldehyde (0.33 ml; 3.46 mmol) as white solid (0.64 g; 95%). Mp 280 °C dec. IR (film, cm^{-1}) $\nu_{\text{max}}=1770$ (C=O), 1730 (C=O); ^1H NMR (400 MHz, DMSO-d_6) $\delta=4.43$ (s, 2H), 7.61–7.66 (m, 1H), 7.89 (s, 1H), 8.02–8.06 (m, 1H), 8.16 (dt, 1H, $J=7.7$, 1.4 Hz), 8.68–8.72 (m, 1H), 11.50 (s, 1H) ppm ^{13}C NMR (100 MHz, DMSO-d_6) $\delta=49.0$, 121.6, 125.2, 139.3, 140.6, 146.8, 150.5, 153.3, 168.7 ppm HRMS (ESI) $[\text{M} + \text{H}]^+$: m/z calcd for ($\text{C}_9\text{H}_9\text{N}_4\text{O}_2$) 205.0726. Found 205.0732.

2.2.14. 1-((Pyridin-3-ylmethylene)amino)imidazolidine-2,4-dione (15)

Compound **15** was prepared according to the general procedure from compound **1** (0.5 g; 3.30 mmol) and pyridine-3-carbaldehyde (0.33 ml; 3.46 mmol) as white solid (0.60 g; 90%). Mp 280 °C dec. IR (film, cm^{-1}) ν_{max} = 1764 (C=O), 1722 (C=O); ^1H NMR (400 MHz, D_2O + NaOH + dioxane) δ = 7.46–7.51 (*m*, 1H), 7.56 (*s*, 1H), 8.18 (*td*, 1H, *J* = 8.0, 1.8 Hz), 8.48 (*dd*, 1H, *J* = 4.9, 1.6 Hz), 8.74 (*d*, 1H, *J* = 1.8 Hz) ppm ^{13}C NMR (100 MHz, D_2O + NaOH + dioxane) δ = 49.3 (*br*), 125.1, 131.6, 135.1, 138.9, 148.1, 149.7, 170.0, 186.3 ppm HRMS (ESI) $[\text{M} + \text{H}]^+$: *m/z* calcd for ($\text{C}_9\text{H}_9\text{N}_4\text{O}_2$) 205.0726. Found 205.0731.

2.2.15. 1-((Pyridin-4-ylmethylene)amino)imidazolidine-2,4-dione (16)

Compound **16** was prepared according to the general procedure from compound **1** (0.5 g; 3.30 mmol) and pyridine-4-carbaldehyde (0.33 ml; 3.46 mmol) as white solid (0.61 g; 91%). Mp 280 °C dec. IR (film, cm^{-1}) ν_{max} = 1750 (C=O), 1723 (C=O); ^1H NMR (400 MHz, D_2O + NaOH + dioxane) δ = 7.46 (*s*, 1H), 7.62–7.66 (*m*, 2H), 8.47–8.51 (*m*, 2H) ppm ^{13}C NMR (100 MHz, D_2O + NaOH + dioxane) δ = 49.3 (*br*), 121.9, 139.2, 143.5, 149.7, 170.0, 186.4 ppm HRMS (ESI) $[\text{M} + \text{H}]^+$: *m/z* calcd for ($\text{C}_9\text{H}_9\text{N}_4\text{O}_2$) 205.0726. Found 205.0730.

2.2.16. 1-(((1*H*-Imidazol-5-yl)methylene)amino)imidazolidine-2,4-dione (17)

Compound **17** was prepared according to the general procedure from compound **1** (0.5 g; 3.30 mmol) and 1*H*-imidazole-5-carbaldehyde (0.33 g; 3.46 mmol) as white solid (0.62 g; 97%). Mp 270 °C dec. IR (film, cm^{-1}) ν_{max} = 1764 (C=O), 1715 (C=O); ^1H NMR (400 MHz, D_2O + NaOH + dioxane) δ = 7.45–7.48 (*m*, 1H), 7.67 (*s*, 1H), 7.72–7.76 (*m*, 1H) ppm ^{13}C NMR (100 MHz, D_2O + NaOH + dioxane) δ = 49.5 (*br*), 125.1, 134.2, 136.5, 140.8, 170.3, 186.7 ppm HRMS (ESI) $[\text{M} + \text{H}]^+$: *m/z* calcd for ($\text{C}_7\text{H}_8\text{N}_5\text{O}_2$) 194.0678. Found 194.0687.

2.3. Ca inhibitory assay

An Applied Photophysics stopped-flow instrument has been used for assaying the CA catalysed CO_2 hydration activity, as reported earlier^{38,39}. The inhibition constants were obtained by non-linear least-squares methods using PRISM 3 and the Cheng-Prusoff equation as reported earlier⁴⁰ and represent the mean from at least

three different determinations. The four tested CA isoforms were recombinant ones obtained in-house as reported earlier^{41–43}.

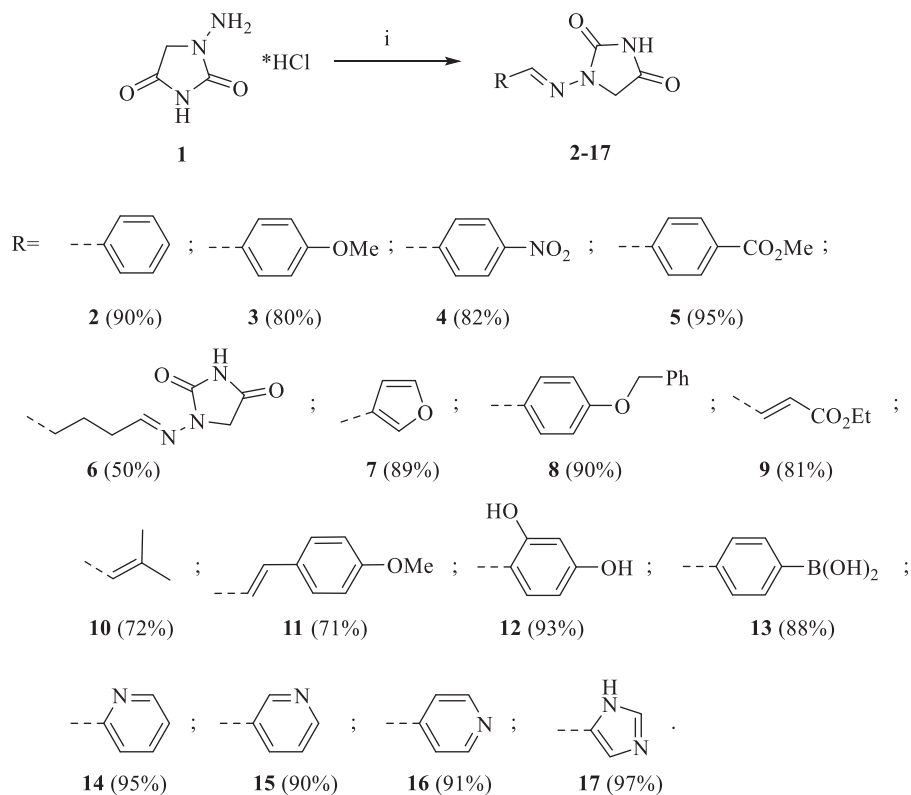
2.4. Computational studies

The crystal structure of CA II (pdb 5LJT)⁴³, CA IX (pdb 5FL4)⁴⁴ and CA XII (pdb JLD0)⁴⁵ were prepared using the Protein Preparation Wizard tool implemented in Maestro - Schrödinger suite, assigning bond orders, adding hydrogens, deleting water molecules, and optimising H-bonding networks⁴⁶. Energy minimisation protocol with a root mean square deviation (RMSD) value of 0.30 was applied using an Optimised Potentials for Liquid Simulation (OPLS3e) force field. 3D ligand structures were prepared by Maestro^{46a} and evaluated for their ionisation states at $\text{pH } 7.4 \pm 0.5$ with Epik^{46b}. Additionally, the imidic nitrogen of the hydantoin nucleus was negatively charged in simulations. OPLS3e force field in MacroModel^{46e} was used for energy minimisation for a maximum number of 2500 conjugate gradient iteration and setting a convergence criterion of $0.05 \text{ kcal mol}^{-1} \text{ \AA}^{-1}$. The docking grid was centred on the centre of mass of the co-crystallized ligands and Glide used with default settings. Ligands were docked with the standard precision mode (SP) of Glide^{46e} and the best 5 poses of each molecule retained as output. The best pose for each compound, evaluated in terms of coordination, hydrogen bond interactions and hydrophobic contacts, was refined with Prime^{46d} with a VSGB solvation model considering the target flexible within 3 Å around the ligand^{47–49}.

The best poses of Furagin and **12** to CA II, CA IX and CA XII were submitted to a MD simulation using Desmond⁵⁰ and the OPL3e force field. Specifically, the system was solvated in an orthorhombic box using TIP4PEW water molecules, extended 15 Å away from any protein atom. It was neutralised adding chlorine and sodium ions. The simulation protocol included a starting relaxation step followed by a final production phase of 100 ns. In particular, the relaxation step comprised the following: (a) a stage of 100 ps at 10K retaining the harmonic restraints on the solute heavy atoms (force constant of $50.0 \text{ kcal mol}^{-1} \text{ \AA}^{-2}$) using the NPT ensemble with Brownian dynamics; (b) a stage of 12 ps at 10K with harmonic restraints on the solute heavy atoms (force constant of $50.0 \text{ kcal mol}^{-1} \text{ \AA}^{-2}$), using the NVT ensemble and Berendsen thermostat; (c) a stage of 12 ps at 10K and 1 atm, retaining the harmonic restraints and using the NPT ensemble and Berendsen thermostat and barostat; (f) a stage of 12 ps at 300 K and 1 atm, retaining the harmonic restraints and using the NPT ensemble and Berendsen thermostat and barostat; (g) a final 24 ps stage at 300 K and 1 atm without harmonic restraints, using the NPT Berendsen thermostat and barostat. The final production phase of MD was run using a canonical NPT Berendsen ensemble at temperature 300 K. During the MD simulation, a time step of 2 fs was used while constraining the bond lengths of hydrogen atoms with the M-SHAKE algorithm. The atomic coordinates of the system were saved every 100 ps along the MD trajectory. Protein and ligand RMSD values, ligand torsions evolution and occupancy of intermolecular hydrogen bonds and hydrophobic contacts were computed along the production phase of the MD simulation with the Simulation Interaction Diagram tools implemented in Maestro.

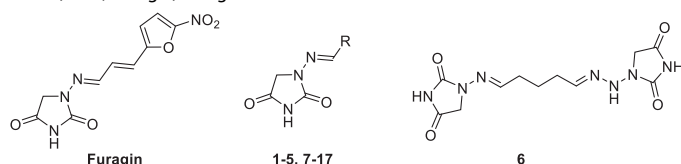
3. Results and discussion**3.1. Chemistry**

A series of Furagin derivatives **2–17** were prepared in reaction between 1-aminohydantoin hydrochloride (**1**) and various



Scheme 1. Reagents and conditions: i. RCHO, EtOH, RT, 16 h

Table 1. Inhibition data of human CA isoforms CA I, II, IX, and XII with aminohydantoin derivatives (2–17, Furagin) using AAZ as a standard inhibitor.



Comp.	R	K_i (nM)*			
		CA I	CA II	CA IX	CA XII
2	C ₆ H ₅	39 600	900	3500	5600
3	4-OCH ₃ -C ₆ H ₄	57 600	6400	1200	4700
4	4-NO ₂ -C ₆ H ₄	>100 000	11 100	7400	2800
5	4-(CO ₂ CH ₃)-C ₆ H ₄	>100 000	8300	4900	930
6	-	19 100	4000	1100	160
7	3-furanyl	16 800	710	850	1700
8	4-(OCH ₂ C ₆ H ₅)-C ₆ H ₄	>100 000	540	350	910
9	CHCH(CO ₂ C ₂ H ₅)	45 900	23 600	810	440
10	CHC(CH ₃) ₂	28 800	16 500	2900	880
11	CHCH(4-OCH ₃ -C ₆ H ₄)	>100 000	3100	400	360
12	2,4-(OH) ₂ -C ₆ H ₃	>100 000	59 900	5800	150
13	4-(B(OH) ₂)-C ₆ H ₄	90 700	14 200	7300	230
14	2-pyridyl	51 800	4200	4500	1300
15	3-pyridyl	45 600	620	2300	3200
16	4-pyridyl	26 600	3300	1600	810
17	5-imidazolyl	9600	12 400	560	350
Furagin	-	>100 000	9600	260	57
AAZ	-	250	12	25	6

*Mean from 3 different assays, by a stopped flow technique (errors were in the range of ± 5 –10% of the reported values).

aldehydes (Scheme 1). Compounds 2–17 were isolated in good to excellent yields, all new structures were proven by ¹H and ¹³C NMR and IR spectroscopy as well as high-resolution mass spectra. The purity of all compounds was greater than 95% according to UPLC analysis.

3.2. Biological evaluation

The CA inhibitory profiles of Furagin and synthesised aminohydantoin derivatives were evaluated by applying a stopped flow carbon dioxide hydrase assay⁵¹, in comparison to acetazolamide (AAZ) as a standard CAI against four physiologically significant isoforms CA I, II, IX, and XII. The following structure–activity relationship (SAR) can be concluded from the inhibition data presented in Table 1.

- All the tested aminohydantoin derivatives exhibited weak inhibitory effect on the slow cytosolic isoform, hCA I, where the binding affinity constant (K_i) values fluctuating in the thousands nM range (K_i 16 800–>100 000 nM).
- The physiologically relevant isoform, hCA II, was better inhibited by most of the tested compounds (K_i s: 620–59 000 nM). It is observed that, the aminohydantoin compounds (2, 7, 8 and 15) were more potent hCA II inhibitors with K_i s in range from 540–900 nM. These compounds have unsubstituted Ph or hetaryl moieties. Rest of the compounds showed weaker inhibitory effect of CA II with K_i s in range from 3100–59 900 nM. It is interesting to note, that compound 12 having dihydroxyphenyl substituent stood out by nearly three times weaker inhibition compare to the second weakest inhibitor 9.
- The tumour associated isoform hCA IX was inhibited in nanomolar range by compounds 7–9, 11, 17 and Furagin (K_i s: 260–850 nM), where the strongest inhibition was observed for Furagin. Rest of the aminohydantoin derivatives showed one order weaker inhibition with K_i s in range from 1100–7 300 nM. Certain pattern can be observed, where better CA IX inhibition can be observed for compounds with vinyl substituents (9, 11, 17 and Furagin) or small hetaryl substituents (7 and 17), with exception in case of compound 8, containing ester moiety on phenyl ring.

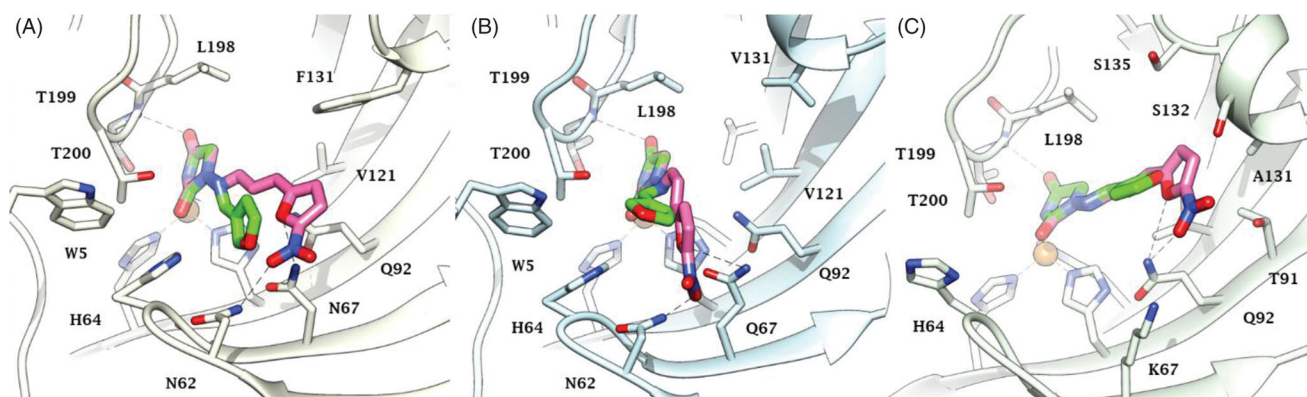


Figure 2. Predicted docking orientations of **7** (green) and **Furagin** (pink) to (A) CA II, (B) CA IX and (C) CA XII.

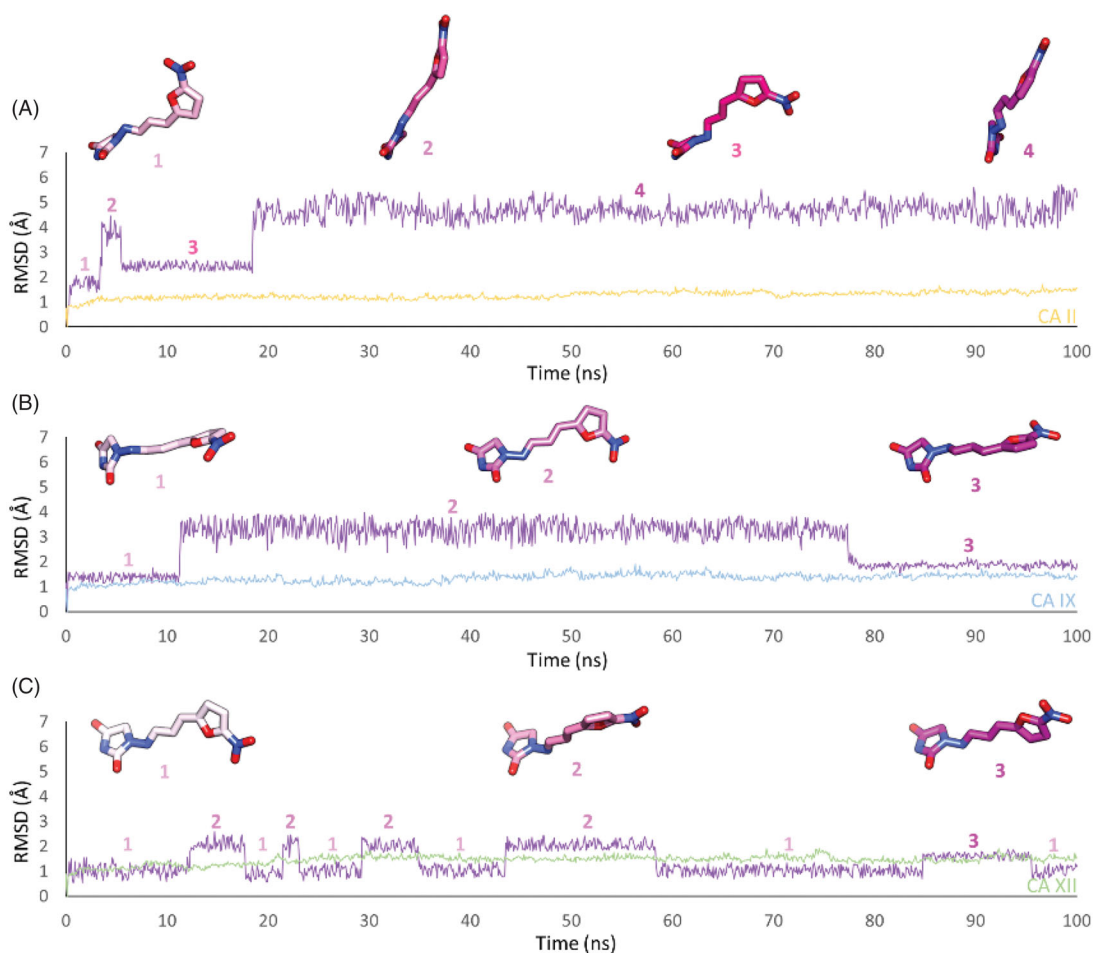


Figure 3. RMSD analysis of **Furagin** heavy atoms and (A) CA II, (B) CA IX and (C) CA XII backbone over the 100 ns MD simulation. The ligand colour darkens over the dynamic simulation.

- d. The other tumour associated isoform hCA XII was best inhibited among all isoforms studied. The best compound of this series was **Furagin** with $K_i = 57$ nM. It was followed by vinyl substituted aminohydantoin derivatives **6**, **9** and **10** with K_i s 160, 360 and 880 nM, respectively. One order weaker CA XII inhibition compare to **Furagin** was also observed for aryl (**5**, **8** and **12**) and hetaryl (**16** and **17**) derivatives ranging K_i s from 150 to 930 nM.

In general good selectivity against cancer associated CA isoforms (CA IX and CA XII) compare to off-target ones (CA I and CA II) was observed for three compounds **Furagin**, **9** and **12**.

3.3. Computational studies

Docking studies were used to investigate the binding mode of **Furagin** and aminohydantoines **2-17** within the active site of CA II (pdb 5LJT)⁴⁴, IX (pdb 5FL4)⁴³ and XII (pdb JLD0)⁴⁵. Similarly to benzenesulfonamides (pKa 10.1) which binds to the CA Zn ion in the deprotonated form, the imidic nitrogen of the hydantoin nucleus as well was considered negatively charged (pKa 9.16)⁵² in the docking experiments and resulted to coordinate the zinc ion in all the obtained poses with CAs II, IX and XII. Furthermore, the oxygen atom of the CO in position 4 of the hydantoin core acts as a bifurcated acceptor establishing two H-bonds with T199, that

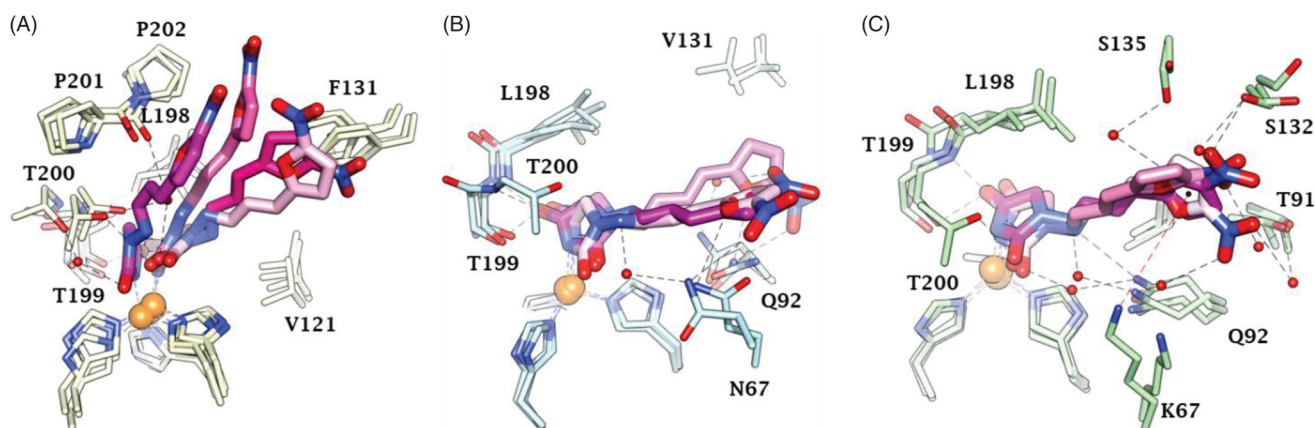


Figure 4. Dynamics evolution of the binding mode of Furagin to (A) CA II, (B) CA IX and (C) CA XII over the course of 100 ns. Water molecules are represented as red spheres. The ligand colour darkens over the dynamic simulation.

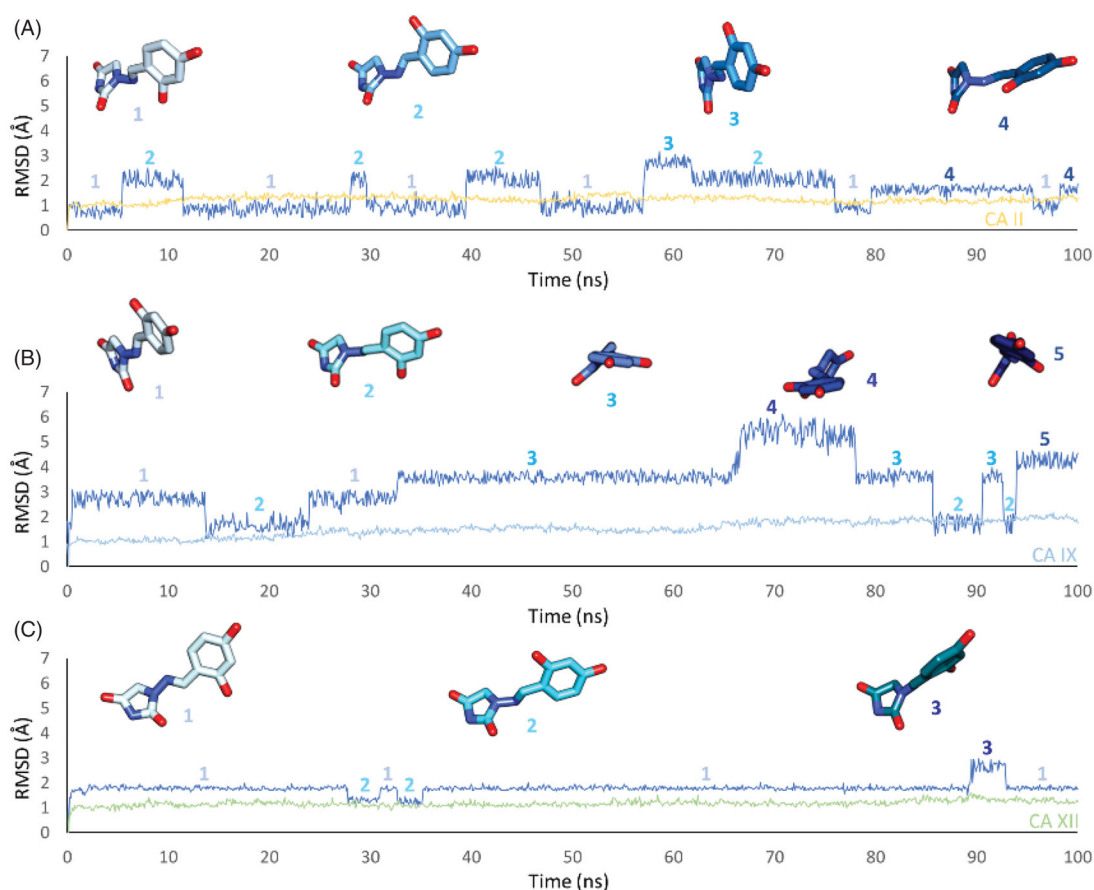


Figure 5. RMSD analysis of 12 heavy atoms and (A) CA II, (B) CA IX and (C) CA XII backbone over the 100 ns MD simulation. The ligand colour darkens over the dynamic simulation.

is, O \cdots (H-N, HG1-O), whereas overall the heterocycle forms VdW contacts with residues H94, H96, H119, L198, T200 and W209 (Figure 2).

In CA II and CA IX, the N₁ pendants of all ligands are oriented towards a hydrophilic cleft defined by H4, W5, N62, N67 and H64, except **8** and **9**, whose N₁ tails are housed, in CA II, into a hydrophobic pocket formed by I91, V121 and F131 (Figure 2(A–B)). Amino acids T91, Q92, A131, S132 and S135 are instead targeted by the pendants on the aminohydantoin of the ligands in all docking solutions with CA XII (Figure 2(C)). The docking procedure was complemented with 100 ns long molecular dynamic (MD)

simulations on the predicted binding conformations of Furagin and **12**, the most potent CA XII inhibitors also showing significant CA XII over CA II selectivity. The structure of the three investigated CA isoforms was stable during the computation with the backbone atom RMSDs exhibiting small fluctuations over the 100 ns (Figures 3 and 5). Additionally, the ZBG of the ligands remains stably anchored to the metal ion all over the MD, with the hydantoin core receiving H-bonds by the amidic NH and side chain OH of Thr199 (Figures 4 and 6).

After an initial equilibration, mainly occurring in CA II and IX, the molecular tail of Furagin undergoes minor conformational

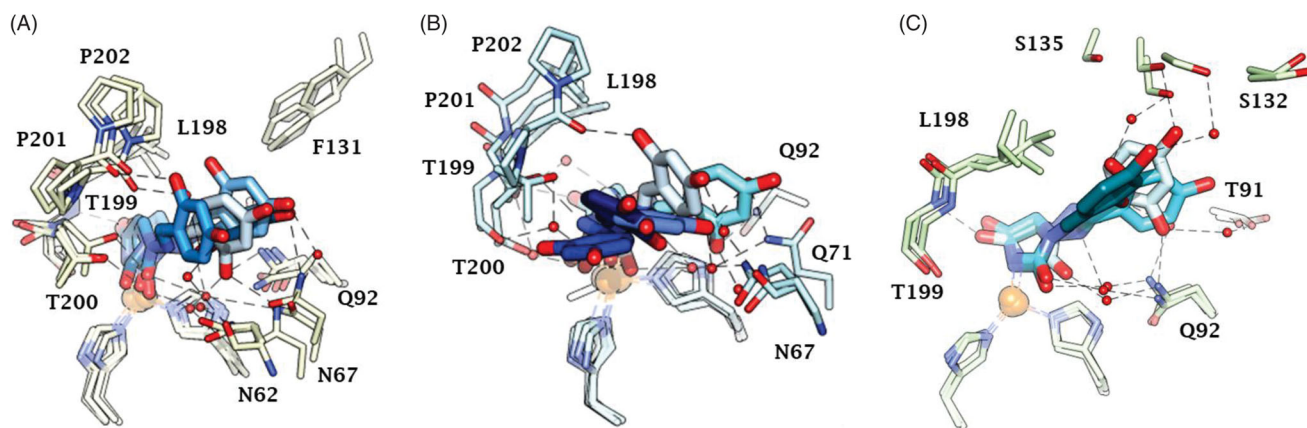


Figure 6. Dynamics evolution of the binding mode of **12** to (A) CA II, (B) CA IX and (C) CA XII over the course of 100 ns. Water molecules are represented as red spheres. The ligand colour darkens over the dynamic simulation.

fluctuations during simulation approaching to stable binding conformations within the three CA isoforms (Figures 3 and 4). In CA IX and XII, the ligand accommodates the N1-pendant in the hydrophilic half of the active sites where it makes VdW contacts and both direct and water mediated H-bond interactions with the enzymes (Figure 4(B,C)). In the CA II, the ligand-bound conformation of Furagin orients the tail towards the hydrophobic area of the target and does not form persistent H-bond interactions over the 100 ns (Figure 4(A)). The hydrogen bond persistence within the three CA isoforms is in good agreement with the inhibitory profile of the ligand (CAXII > CA IX > CA II).

An ensemble of few conformations is representative of the binding of **12** within CA II and IX (Figures 5 and 6). Here, the ligand approaches the hydrophobic regions of the enzymes and, coming next to the end of the simulation, the N₁ tails lose direct or water-bridged H-bonds with glutamine and asparagine residues, progressively moving towards T199 or T200, that is, the area of the enzyme that undergoes to the greatest residue displacement. In CA XII, the docked pose of **12** remains firmly anchored to the residues of the hydrophilic portion of the enzyme throughout the dynamic. A wide network of direct and water mediated H-bonds stabilise the binding of the ligand. This is consistent with the inhibition profile exhibited by **12** in CA XII as compared with the other two CA isoforms.

4. Conclusions

In summary, we have demonstrated that clinically used antibiotic – Furagin and its derivatives **2-17** are potential CA inhibitors. Furagin and all newly synthesised hydantoin derivative were examined for their inhibitory activities towards hCA I, II, IX and XII. The four studied hCA isoforms were inhibited by Furagin and its derivatives at various degrees. In particular, Furagin and prepared compounds **2-17** did not inhibit or poorly inhibited off-target hCA I with K_i s ranging from >100 μ M (compounds **4**, **5**, **8**, **11**, **12** and Furagin) to 9.6 μ M. Ubiquitous hCA II was poorly inhibited by compounds **3-6**, **9-14**, **16**, **17** and Furagin (K_i s from 59.9 to 3.1 μ M). Rest of the compounds significantly inhibited hCA II (K_i s from 900 nM to 540 nM). Remarkable inhibition of cancer associated hCA IX was observed for Furagin (K_i =260 nM) and compounds **7-9**, **11** and **17** with K_i s ranging from 350 to 850 nM. The rest of compounds exhibited slightly weaker inhibition of hCA IX with K_i s ranging from 1100 to 7400 nM. Other cancer associated isoform – hCA XII also was significantly inhibited by Furagin (K_i =57 nM) and compounds **5**, **6**, **8-13**, **16** and **17** (K_i s from 160 to

910 nM). The rest of the compounds exhibited slightly weaker inhibition with K_i s ranging from 1300 to 5600 nM. Docking and molecular dynamics simulations shed light on the ligands selectivity for the cancer-associated CAs over ubiquitous CA II. The significant inhibition activity and especially selectivity of Furagin against hCA IX and XII was attributed due to the strong H-bond interactions, whereas in case of hCA II no persistent H-bond interactions are formed due to Furagin's tails orientation towards hydrophobic area of the enzyme.

The knowledge obtained gives the solid base for both – investigation of drug repurposing of clinically used antibiotic Furagin for anti-cancer therapy and further studies of new chemotype of inhibitors of CAs.

Disclosure statement

The authors have no relevant affiliations of financial involvement with any organisation or entity with a financial interest in or financial conflict with the subject matter or materials discussed in the manuscript.

ORCID

Claudiu T. Supuran  <http://orcid.org/0000-0003-4262-0323>

References

- Supuran CT. Structure and function of carbonic anhydrases. *Biochem J* 2016;473:2023–32.
- Alterio V, Di Fiore A, D'Ambrosio K, et al. Multiple binding modes of inhibitors to carbonic anhydrases: how to design specific drugs targeting 15 different isoforms. *Chem Rev* 2012;112:4421–68.
- Supuran CT. Carbonic anhydrases: novel therapeutic applications for inhibitors and activators. *Nature Rev Drug Discov* 2008;7:168–81.
- Jensen EL, Clement R, Kosta A, et al. A new widespread subclass of carbonic anhydrase in marine phytoplankton. *Isme J* 2019;13:2094–106.
- Del Prete S, Vullo D, Fisher GM, et al. Discovery of a new family of carbonic anhydrases in the malaria pathogen *Plasmodium falciparum* – the η -carbonic anhydrases. *Bioorg Med Chem Lett* 2014;24:4389–96.

6. Xu Y, Feng L, Jeffrey PD, et al. Structure and metal exchange in the cadmium carbonic anhydrase of marine diatoms. *Nature* 2008;452:56–61.
7. Supuran CT, Capasso C. Biomedical applications of prokaryotic carbonic anhydrases. *Expert Opin Ther Pat* 2018;28:745–54.
8. Capasso C, Supuran CT. An overview of the alpha-, beta- and gamma-carbonic anhydrases from bacteria: can bacterial carbonic anhydrases shed new light on evolution of bacteria?. *J Enzyme Inhib Med Chem* 2015;30:325–32.
9. Capasso C, Supuran CT. Bacterial, fungal and protozoan carbonic anhydrases as drug targets. *Expert Opin Ther Targets* 2015;19:1689–704.
10. Capasso C, Supuran CT. Anti-infective carbonic anhydrase inhibitors: a patent and literature review. *Expert Opin Ther Pat* 2013;23:693–704.
11. Nocentini A, Supuran CT. Advances in the structural annotation of human carbonic anhydrases and impact on future drug discovery. *Expert Opin Drug Discov* 2019;14:1175–97.
12. Supuran CT. Advances in structure-based drug discovery of carbonic anhydrase inhibitors. *Expert Opin Drug Discov* 2017;12:61–88.
13. Supuran CT. How many carbonic anhydrase inhibition mechanisms exist?. *J Enzyme Inhib Med Chem* 2016;31:345–60.
14. De Simone G, Supuran CT. (In)organic anions as carbonic anhydrase inhibitors. *J Inorg Biochem* 2012;111:117–29.
15. Supuran CT. Carbonic anhydrase inhibitors as emerging agents for the treatment and imaging of hypoxic tumors. *Expert Opin Investig Drugs* 2018;27:963–70.
16. Supuran CT. Carbonic anhydrase inhibitors and their potential in a range of therapeutic areas. *Expert Opin Ther Pat* 2018;28:709–12.
17. Supuran CT. Applications of carbonic anhydrases inhibitors in renal and central nervous system diseases. *Expert Opin Ther Pat* 2018;28:713–21.
18. Supuran CT, Alterio V, Di Fiore A, et al. Inhibition of carbonic anhydrase IX targets primary tumors, metastases, and cancer stem cells: three for the price of one. *Med Res Rev* 2018;38:1799–836.
19. Neri D, Supuran CT. Interfering with pH regulation in tumours as a therapeutic strategy. *Nat Rev Drug Discov* 2011;10:767–77.
20. Da'dara AA, Angeli A, Ferraroni M, et al. Crystal structure and chemical inhibition of essential schistosome host-interactive virulence factor carbonic anhydrase SmCA. *Commun Biol* 2019;2:333.
21. Supuran CT. Carbonic anhydrases and metabolism. *Metabolites* 2018;8:25.
22. Supuran CT. Carbonic anhydrase inhibition and the management of hypoxic tumors. *Metabolites* 2017;7:E48.
23. Tars K, Vullo D, Kazaks A, et al. Sulfocoumarins (1,2-benzoxathiine 2,2-dioxides): a class of potent and isoform-selective inhibitors of tumor-associated carbonic anhydrases. *J Med Chem* 2013;56:293–300.
24. Nocentini A, Ceruso M, Carta F, et al. 7-Aryl-triazolyl-substituted sulfocoumarins are potent, selective inhibitors of the tumor-associated carbonic anhydrase IX and XII. *J Enzyme Inhib Med Chem* 2016;31:1226–33.
25. Grandane A, Tanc M, Di Cesare Mannelli L, et al. Substituted sulfocoumarins are selective carbonic anhydrase IX and XII inhibitors with significant cytotoxicity against colorectal cancer cells. *J Med Chem* 2015;58:3975–83.
26. Tanc M, Carta F, Bozdog M, et al. 7-Substituted-sulfocoumarins are isoform-selective, potent carbonic anhydrase II inhibitors. *Bioorg Med Chem* 2013;21:4502–10.
27. Touisni N, Maresca A, McDonald PC, et al. Glycosylcoumarin carbonic anhydrase IX and XII inhibitors strongly attenuate the growth of primary breast tumors. *J Med Chem* 2011;54:8271–7.
28. Maresca A, Temperini C, Pochet L, et al. Deciphering the mechanism of carbonic anhydrase inhibition with coumarins and thiocoumarins. *J Med Chem* 2010;53:335–44.
29. Temperini C, Innocenti A, Scozzafava A, et al. The coumarin binding site in carbonic anhydrase accommodates structurally diverse inhibitors: the antiepileptic lacosamide as an example. *J Med Chem* 2010;53:850–4.
30. Maresca A, Temperini C, Vu H, et al. Non-zinc mediated inhibition of carbonic anhydrases: coumarins are a new class of suicide inhibitors. *J Am Chem Soc* 2009;131:3057–62.
31. Pustenko A, Stepanovs D, Žalubovskis R, et al. 3H-1,2-benzoxathiepine 2,2-dioxides: a new class of isoform-selective carbonic anhydrase inhibitors. *J Enzyme Inhib Med Chem* 2017;32:767–75.
32. Ivanova J, Carta F, Vullo D, et al. N-Substituted and ring opened saccharin derivatives selectively inhibit transmembrane, tumor-associated carbonic anhydrases IX and XII. *Bioorg Med Chem* 2017;25:3583–9.
33. Alterio V, Tanc M, Ivanova J, et al. X-ray crystallographic and kinetic investigations of 6-sulfamoyl-saccharin as a carbonic anhydrase inhibitor. *Org Biomol Chem* 2015;13:4064–9.
34. Ivanova J, Leitans J, Tanc M, et al. X-ray crystallography-promoted drug design of carbonic anhydrase inhibitors. *Chem Commun (Camb)* 2015;51:7108–11.
35. Chernov NM, Koshevenko AS, Yakovlev IP, et al. Synthesis and antimicrobial activity of 4-hydroxy-2-[5-nitrofuranyl-2-yl]-6h-1,3-oxazin-6-ones. *Pharm Chem J* 2017;51:644–7.
36. Gut J, Novacek A, Fiedler P. Reaction of six-membered cyclic hydrazides with aromatic aldehydes. *Collect Czechoslovak Chem Comm* 1968;33:2087–96.
37. Wang Q, Liu Y-C, Chen Y-J, et al. Development of a direct competitive chemiluminescent ELISA for the detection of nitrofurantoin metabolite 1-amino-hydantoin in fish and honey. *Anal Methods* 2014;6:4414–20.
38. Nocentini A, Ceruso M, Bua S, et al. Discovery of β -adrenergic receptors blocker-carbonic anhydrase inhibitor hybrids for multitargeted antiglaucoma therapy. *J Med Chem* 2018;61:5380–94.
39. Köhler K, Hillebrecht A, Schulze Wischeler J, et al. Saccharin inhibits carbonic anhydrases: possible explanation for its unpleasant metallic aftertaste. *Angew Chem Int Ed Engl* 2007;46:7697–9.
40. Eldehna WM, Nocentini A, Bonardi A, et al. 3-Hydrazinoisatin-based benzenesulfonamides as novel carbonic anhydrase inhibitors endowed with anticancer activity: Synthesis, *in vitro* biological evaluation and *in silico* insights. *Eur J Med Chem* 2019;184:111768.
41. Eldehna WM, Nocentini A, Al-Rashood ST, et al. Tumor-associated carbonic anhydrase isoform IX and XII inhibitory properties of certain isatin-bearing sulfonamides endowed with *in vitro* antitumor activity towards colon cancer. *Bioorg Chem* 2018;81:425–32.
42. Al-Sanea MM, Elkamhawry A, Paik S, et al. Synthesis and biological evaluation of novel 3-(quinolin-4-ylamino)benzenesulfonamides as carbonic anhydrase isoforms I and II inhibitors. *J Enzyme Inhib Med Chem* 2019;34:1457–64.

43. Leitans J, Kazaks A, Balode A, et al. Efficient expression and crystallization system of cancer-associated carbonic anhydrase isoform IX. *J Med Chem* 2015;58:9004–9.
44. Nocentini A, Ferraroni M, Carta F, et al. Benzenesulfonamides incorporating flexible Triazole moieties are highly effective carbonic anhydrase inhibitors: synthesis and kinetic, crystallographic, computational, and intraocular pressure lowering investigations. *J Med Chem* 2016;59:10692–704.
45. Whittington DA, Waheed A, Ulmasov B, et al. Crystal structure of the dimeric extracellular domain of human carbonic anhydrase XII, a bitopic membrane protein overexpressed in certain cancer tumor cells. *Proc Natl Acad Sci USA* 2001;98:9545–50.
46. Schrödinger Suite Release 2019-1, Schrödinger, LLC, New York, NY, 2019: (a) Prime, v.5.5; Maestro v.11.9; (b) Epik, v.4.7; (c) Impact, v.8.2; (d) Macromodel v.12.3. (e) Glide, v.8.2.
47. (a) Nocentini A, Gratteri P, Supuran CT. Phosphorus versus Sulfur: Discovery of Benzenephosphonamidates as Versatile Sulfonamide-Mimic Chemotypes Acting as Carbonic Anhydrase Inhibitors. *Chemistry* 2019;25:1188–92. (b) Supuran CT. Carbon- versus sulphur-based zinc binding groups for carbonic anhydrase inhibitors? *J Enzyme Inhib Med Chem* 2018;33:485–95. 33: 485–95.
48. Nocentini A, Bonardi A, Gratteri P, et al. Steroids interfere with human carbonic anhydrase activity by using alternative binding mechanisms. *J Enzyme Inhib Med Chem* 2018;33:1453–9.
49. Nocentini A, Carta F, Tanc M, et al. Deciphering the mechanism of human carbonic anhydrases inhibition with sulfocoumarins: computational and experimental studies. *Chemistry* 2018;24:7840–4.
50. Schrödinger Release 2019-2: Desmond Molecular Dynamics System, D. E. Shaw Research, New York, NY, 2019, v.5.7.
51. Khalifah RG. The carbon dioxide hydration activity of carbonic anhydrase. I. Stop-flow kinetic studies on the native human isoenzymes B and C. *J Biol Chem* 1971;246:2561–73.
52. Verdolino V, Cammi R, Munk BH, et al. Calculation of pKa values of nucleobases and the guanine oxidation products guanidinohydantoin and spiroiminodihydantoin using density functional theory and a polarizable continuum model. *J Phys Chem B* 2008;112:16860–73.